J. Fluid Mech. (2007), *vol.* 573, *pp.* 297–310.
doi:10.1017/S0022112006003983 Printed in the United Kingdom

Slow rupture of viscous films between parallel needles

SOFYA V. CHEPUSHTANOVA
AND IGOR L. KLIAKHANDLER

Department of Mathematical Sciences, Michigan Technological University,
1400 Townsend Drive, Houghton, MI 49931-1295, USA

(Received 17 November 2005 and in revised form 5 August 2006)

Experiments and theory on the rupture of a free plane viscous film are reported. The relatively thick film, with a typical thickness of the order of 0.1–0.6 mm, rests between two long parallel needles. When the film is punctured, a hole is formed with the rim on the front. The hole expands, reaches the needles, and propagates along them with a constant velocity of the order of 2–50 cm s^{-1}. The Reynolds numbers for the present experiments are relatively small, $0.002 \leqslant Re \leqslant 0.34$. A crude theory for propagation velocity of the rim is proposed; the theory compares well with the experimental data. The rupture profile is visually similar to a U-shaped curve. Crude equations for the rupture profile are derived, and their solutions are consistent with the experimental observations. A theory for propagation velocity and profile of the rupture, applicable to all Reynolds numbers, is proposed.

1. Introduction

Soap films and their rupture are universally familiar and, because of their visual simplicity, attracted scientific attention more than a century ago. In an idealized setting, the punctured film develops an expanding radial hole with a rim, which collects the liquid. The film far from the rim remains undisturbed.

The first study of the inviscid soap-film rupture in such a setting was conducted by Dupré (1867). Using energy balance, he obtained an expression for the rim velocity $U = (4\sigma/\rho h)^{1/2}$, independent of the radius of the hole. Here, σ is the surface tension, ρ is the liquid density, and h is the initial thickness of the film at rest. Rayleigh (1891) studied the rupturing process of a soap film experimentally and found that his results generally agreed with Dupré's theory.

More sophisticated experiments were conducted by Ranz (1959). His results showed that actual film edge velocity is about 10 % lower than that predicted by Dupré's formula. Further analyses, made independently by Taylor (1959) and Culick (1960), gave a somewhat different result: using the correct momentum balance, they both found that the hole in the soap film grows at the rate

$$U_{TC} = \left(\frac{2\sigma}{\rho h}\right)^{1/2}. \tag{1}$$

This is $1/\sqrt{2}$ smaller than that computed by Dupré and Ranz. The validity of this formula has been confirmed experimentally McEntree & Mysels (1969). Keller (1983) proposed some extension of the Taylor–Culick momentum balance theory to non-uniform threads and films and analysed the influence of various parameters on the motion of the rim.

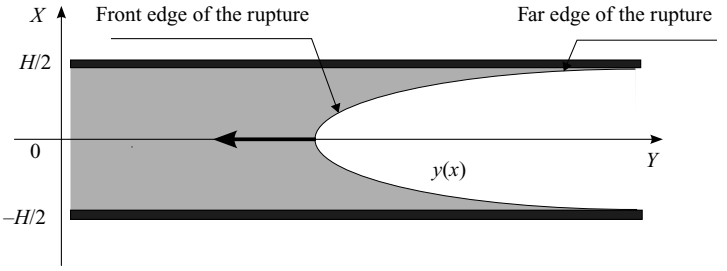

FIGURE 1. Schematic view of the rupture front between two needles.

The dynamics of a rupturing soap film was also observed and discussed in detail by Pandit & Davidson (1990). They measured the liquid-film thickness and velocity of the moving rim. Taking into account the previous work, Pandit & Davidson (1990) proposed two alternative methods for obtaining a formula for rim velocity – momentum balance and energy balance, with the same formula, (1), as Taylor (1959) and Culick (1960).

The subject of the papers mentioned above, is the rupture of *inviscid* (soap) films and propagation of the circular rim, with a typical high Reynolds number. The rupture of *viscous* plane films was considered in another group of papers. The first observations of the disintegration of very viscous (viscoelastic) liquid films are reported by Debrégeas, Martin & Brochard-Wyard (1995) and Debrégeas, de Gennes & Brochard-Wyard (1998). The new feature, caused by viscous dissipation, is that after being punctured, the liquid from the circular hole is not collected into a rim as it is in soap films. Instead, the liquid spreads out with a thickness that increases uniformly in time. The retraction radius and velocity grow exponentially with rise time $\mu h/2\sigma$, where μ is the viscosity of the film. Brenner & Gueyffier (1999) considered the retraction of a viscous (not viscoelastic) finite-length one-dimensional film. They demonstrated that a ruptured film may or may not have a rim, depending on its Reynolds number Re and length L. For fixed L and $Re \gg 1$, the rim exists and grows with time; the rim velocity is governed by the Taylor–Culick equation (1). For small L (smaller that Stokes length $\mu/\rho U_{TC}$) and $Re \ll 1$, the rim disappears, and the film thickness grows uniformly with time. This means that the viscous effects have an impact on the entire liquid film.

Sünderhauf, Raszillier & Durst (2002) investigated the dynamical acceleration of the free two-dimensional edge of a liquid sheet toward the Taylor–Culick limit. Their numerical simulations show images and features of the thickening film and streamlines of the flow, for both high and low viscosity. For the low-viscosity regime, they find that global momentum balance describes the velocity of contraction quite well. For large viscosity, the rim extends into the liquid (in accordance with the results of Brenner & Gueyffier 1999). They conclude that, for large times, the velocity of the thickening rim always approaches the Taylor–Culick limit, (1). The results are applied to the stability of liquid curtains. Also, Adachi *et al.* (1998) obtained the steady shape of a free edge in a vertical liquid curtain in the inertia-dominated regime, and demonstrated the impact of rim weight on the shape of the edge.

In this study, rupture of a viscous film between two parallel needles is considered. Figure 1 shows a schematic of the experiment, and experimental results are shown in figure 2. Unidirectional stationary propagation of the rupture front and retention of liquid on the needles are different from the circular geometry or unidirectional propagation of the thickening edge of the film, as considered in most previous studies.

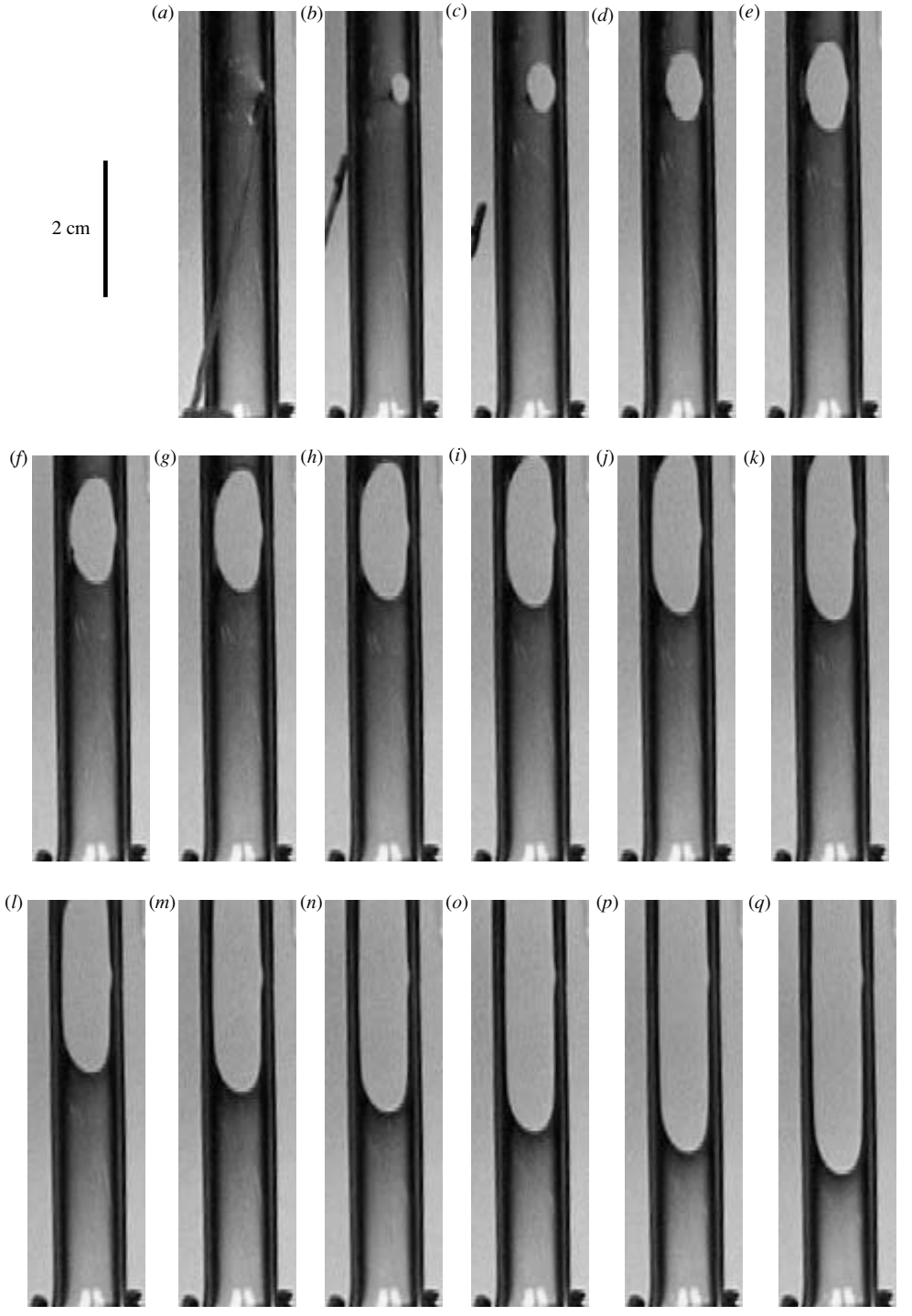

FIGURE 2. Initial and developed stages of the rupture of the viscous film between the needles. The images (*a*)–(*l*) are 0.2 s apart; the images (*l*)–(*q*) are 0.6 s apart.

Visually, the system resembles such classic flows as the rise of long bubbles in a tube (Bretherton 1961), or the unstable displacement fingers in the Hele-Shaw cell (Saffman & Taylor 1958). Similar to the impact of solid walls during the rise of a long bubble in a tube (Bretherton 1961), the needles, loosely speaking, play the role of solid boundaries for the flow. Viscous shear on them arrests the impact of surface tension on the rim. As a result, the rupture propagates with a constant velocity in a steady-state mode with a rim being formed on the rupture front.

A somewhat similar low-viscosity unidirectional soap/glycerol system was mentioned briefly by Liebman, Corry & Pierlee (1968). Though, in general, in their experiments, the front was somewhat unstable and produced many very small drops, it was found that rupture reaches a steady-state mode of propagation and propagates faster for thinner films and larger separation between the needles. However, many details of the process have not been studied; this is the subject of the present paper. A steady-state mode allows us to develop a simple crude averaged theory for propagation velocity and for the U-shaped profile of the rupture front, applicable to all Reynolds numbers. The developed theory for the velocity propagation agrees well with the experiments. The crude theory for the U-shaped profile of the rupture front also gives good argeement with the experiment, though it is harder to ascertain the validity of the theory. It is essential that the Reynolds numbers for the present experiments are relatively small, $0.002 \leqslant Re \leqslant 0.34$. It seems that in all previous experiments with soap films, the Reynolds numbers have been much larger. It would be interesting to evaluate experimentally the validity of the new proposed theories for intermediate (moderately large) Reynolds numbers, i.e. for thin low-viscosity films.

2. Experiments

The photographs in figure 2, taken from above and somewhat to the right-hand side of the film, show our experimental system and the dynamics of the rupture. Two horizontal metal needles, each about 1 mm thick, initially touch each other. The needles are wetted with a viscous liquid between them. After initial experimentation with organic and aqueous liquids, organic fluids have been chosen. The reason is that aqueous liquid films are prone to contamination and develop Marangoni flows which generate holes in the film. Another reason for choosing organic fluids is that they do not evaporate like soap films; this allows us to conduct more reproducible, reliable and controllable experiments.

After a number of preliminary experiments with different organic liquids, it was found that polybutenes were the most suitable for our set-up. Polybutenes, as well as silicone oils, are viscous transparent Newtonian liquids. In our experiments, the polybutenes were coloured to make thin films clearly visible. The dynamic viscosities μ of the liquids are in the range $1000 < \mu < 13\,000$ cP. The viscosities were measured with the Brookfield Digital Viscometer DV-II+ (version 3.0) in the Transportation Materials Research Center laboratory at Michigan Technological University. The measurement error of μ was of the order of 2 %. The surface tension σ of the samples is $0.030 \pm 2\,\mathrm{N\,m^{-1}}$, the density ρ is $0.88 \pm 1\,\mathrm{g\,cm^{-3}}$.

To form a film, the needles were separated by a distance H after being wetted. The resulting film of thickness h is similar to a soap film on a frame. The organic films are, however, substantially thicker and more viscous than soap films. The typical thickness h of viscous films in our experiments is of the order of 10^{-1} mm (see table 1), whereas soap films have a thickness of the order of 10^{-2}–10^{-3} mm (e.g. see Ranz 1959). Typical viscosity of the soap film, being comparable with water viscosity, is of the order of

Liquid	Viscosity μ (cP)	Surface tension σ ($N\,m^{-1}$)	Distance H (cm)	Initial thickness h (mm)	Measured velocity U_μ ($cm\,s^{-1}$)	Calculated velocity U_μ ($cm\,s^{-1}$)	Reynolds number Re
A	1400 ± 25	0.030 ± 2	1.6	0.15 ± 1	37.0 ± 2.0	40	0.34
A	1400 ± 25	0.030 ± 2	1.6	0.61 ± 3	18.4 ± 1.0	19.5	0.34
B	4000 ± 70	0.030 ± 2	1.1	0.10 ± 1	14.2 ± 0.8	13.9	0.03
B	4000 ± 70	0.030 ± 2	1.06	0.23 ± 2	8.6 ± 0.5	9.1	0.03
C	7500 ± 100	0.030 ± 2	0.9	0.12 ± 1	5.9 ± 0.3	6.1	0.007
C	7500 ± 100	0.030 ± 2	1.85	0.12 ± 1	9.2 ± 0.6	8.8	0.014
D	$13\,200 \pm 150$	0.030 ± 2	0.9	0.4 ± 4	1.75 ± 0.1	1.9	0.002
D	$13\,200 \pm 150$	0.030 ± 2	1.8	0.2 ± 2	3.5 ± 0.3	3.8	0.004

TABLE 1. Measurements of all the parameters involved. Liquids A–D are coloured grades of Indopol polybutene of H series.

1 cP, whereas viscosity of the liquids used in our experiments is of the order of a few thousand cP.

The most complicated and delicate part of the experiments was the evaluation of the film thickness h. The film was ruptured immediately after the needles had been separated to a distance H. Otherwise, over time, the levitating film tends to form drops on its lower surface owing to the gravity. So, the measurements of the film thickness at rest, independent of the rupture dynamics, were found to be less controllable. Moreover, formation of the drops is a limiting factor that does not allow us to use low-viscosity liquids in such a horizontal set-up. To measure the film thickness in dynamics, a number of film samples with pre-measured thicknesses were prepared. Each film sample was formed by the deposition of a small amount ($0.1\,cm^3$) of a coloured liquid between two thin transparent pieces of glass. Then the pieces of glass were squeezed, and the circular area occupied by the film was measured. So, given the volume and area of each film sample, it was possible to find its thickness with an error of less then 5 %. Further, to find the thickness h of the rupturing coloured film, the entire experiment was digitally recorded in a controlled lighting environment with pieces of coated glass as controls. The thickness of the dynamically rupturing coloured film was then found by comparison of the optical density of the deposited resting films with the optical density of the rupturing film. The technique is similar to the method used by Vorobieff, Rivera & Ecke (1999).

As a result, prior to the rupture, each film is characterized by the following parameters: thickness h, distance between the needles H, surface tension σ, viscosity μ, and density ρ. Several methods of film puncturing were tried. Usually, a thin metal needle was used. The needle is clearly seen in figure 2(*a–c*).

Typically, the film was punctured in the middle between the needles. Regardless of the puncturing method, it was observed that the system 'forgets' the details of rupturing and reaches the steady-state propagation mode after the moving front edge, or rim, has run a distance of about $(3 - 4)H$. This is clearly seen on figure 2. In figure 2, the film was intentionally punctured near the right-hand needle (figure 2*a–e*), to demonstrate that details of the puncturing are not important for subsequent dynamics: structure of the rupture equilibrates quite fast.

Propagation of the rupture has a few stages (figure 2). At the initial stage of propagation before reaching the needles, the rim collects the liquid in front of it and thickens. The needles are immobile in space, and surface tension, diminishing the free surface area of the film, 'pulls' the liquid toward the needles. After the rim reaches both needles, its thickness stabilizes. This occurs because of the dynamic equilibrium of two processes: collection of the liquid by the moving rim and simultaneous retention of the liquid on the needles. (Retention of the liquid on the needles is the reason why the needles look thicker than they are.) Such equilibrium of mass dynamics leads to the constant velocity propagation mode. Far ahead of the rim, the film remains undisturbed and motionless. The rim is clearly seen during the motion, though the resolution of the digital camera used does not allow its precise measurements (see a darker area on the front of the rupture on figure 2 and on figure 5 below).

During the propagation process, a U-shaped profile is formed in the horizontal plane. The rupture propagates with constant velocity U_μ in a steady-state mode with a steady profile along the needles, until the film breaks up completely. Velocity U_μ was measured through the processing of digital video records of the experiments.

Study of the digital images showed that the film thickness was quite homogeneous. In the least controllable cases, the local maximal non-homogeneity of the film thickness could reach up to 20 %. Note in this respect that the same order of non-homogeneity (about 20 %) of the film thickness was observed in the experiments with soap films by Ranz (1959).

Many experiments with various liquids, colourizations, thicknesses and separation distances were conducted to create the most controllable experimental environment. Generally, the adopted experimental technique turned out to be reliable. Typical results of the experiments are given in table 1.

It was observed that rupture propagates faster for thinner films, wider distances between the needles, and less viscous liquids. Notice also that the needles are substantially thicker than the film itself. It seems therefore that change of needle thickness would not affect the velocity of rupture propagation, but this was not checked experimentally.

3. Theory

3.1. *Dimensional analysis*

Generally, the following six parameters characterize the entire system: U, H, h, σ, μ, ρ. It turns out that three independent dimensionless parameters may be formed from those variables. In particular, a natural choice of parameters is capillary number $Ca = \mu U/\sigma$, Weber number $W = U^2\rho h/\sigma$, and geometric ratio h/H.

When viscosity is small, the rupture process is driven by inertia, viscosity is excluded from the set of essential parameters, and only two dimensionless parameters remain for description of the inertia-dominated regime: geometric ratio h/H and Weber number $U^2\rho h/\sigma$. It can be assumed, in the usual spirit of dimensional analysis, that one of these parameters is a function of the other:

$$W = \frac{U^2\rho h}{\sigma} = G\left[\frac{h}{H}\right]. \tag{2}$$

To evaluate the character of the function G, notice that across the thin levitating film the pressure is constant and equal to the atmospheric pressure. Therefore, in such an inertia-dominated regime, away from the rim, the liquid particles do not interact with each other (pressure is constant), and are 'unaware' of the external size of the system

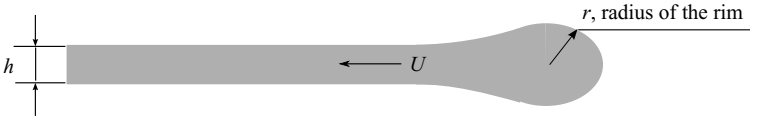

FIGURE 3. The cross-sectional profile of the rim during the rupture process.

H. This means that the velocity of the rupture propagation does not depend on H. Hence, function G in the right-hand side of (2) is, in fact, constant, independent of the geometric ratio h/H. This naturally leads to the Taylor–Culick formula, (1), for velocity, with constant G being equal to 2.

The experiments described above are, however, for the viscosity-dominated regime and can be considered under the assumption of negligible inertia. Small inertia may be interpreted as an indication that ρ is not an important parameter. So, we can assume that, in fact, only five parameters U, H, h, σ, μ characterize the slow rupture of the film, and only two dimensionless parameters remain for description of the viscosity-dominated regime: capillary number $\mu U/\sigma$ and h/H. As previously, it can be assumed that one of those parameters is a function of the other:

$$Ca = \frac{\mu U}{\sigma} = F\left[\frac{h}{H}\right], \quad U = \frac{\sigma}{\mu} F\left[\frac{h}{H}\right]. \tag{3}$$

Note that both for the diminishing thickness h of the film, and for the increasing distance H between the needles, the rupture propagates faster (this was also found in experiments by Liebman *et al.* 1968). This means that $F'(x) < 0$. Notice at the same time that typically $h \ll H$. So, in fact, only the asymptotic regime $h/H \ll 1$ is considered in the present study. It may be assumed that in such an asymptotic limit $h/H \to 0$, function $F(h/H)$ acquires a power form $F(h/H) = (h/H)^{\alpha}$ (Barenblatt 1996). This assumption will be verified in § 3.3.

This dimensional analysis allows us to anticipate the results of more precise considerations below.

3.2. *Rim thickness*

The propagation velocity U_{μ} will be found in the next section through the forces balance. Capillarity is one of the crucial forces in the system. To evaluate the capillary impact, we assume that the rim has a quasi-circular cross-sectional profile of characteristic radius r (figure 3).

For evaluation of the rim radius r, we shall use gross mass balance. To do that, it is necessary to evaluate the typical extent δ of the region in front of the rim, in which the acceleration of the fluid, and hence energy dissipation, occur. The next consideration closely follows the classic arguments by Culick (1960). We suppose that the acceleration of the fluid takes place within a distance δ in front of the rim where the film thickness is approximately h, which is not valid very close to the needles. The volume, where the energy dissipation occurs, is roughly equal to $Hh\delta$. The rate at which the energy is dissipated is of the order of

$$\mu \int \left(\frac{\mathrm{d}v}{\mathrm{d}x}\right)^2 \mathrm{d}x, \tag{4}$$

where the integral is taken over volume (Landau & Lifshitz 1959), and v is the flow field of the system. Since $\mathrm{d}v/\mathrm{d}x \simeq U_{\mu}/\delta$, the approximate value of the integral is about $\mu(U_{\mu}/\delta)^2 Hh\delta$. In the typical soap-film system, half of the surface tension energy is

dissipated, and half goes toward the increase of kinetic energy of the thickening rim, as was stressed by Taylor (1959) and Culick (1960). In the viscous film considered in the present paper, there is no increase in the kinetic energy of the moving film owing to the stationary character of the flow. Therefore, all the surface energy in the system is dissipated. Hence, the rate of the energy dissipation is equal to the rate at which surface energy in the system is released (and not to its half, as in analyses by Taylor 1959 and Culick 1960). The latter is equal to the surface tension multiplied by the rate at which surface area disappears, $2\sigma U_\mu H$. This results in the following:

$$\mu\left(\frac{U_\mu}{\delta}\right)^2 Hh\delta = 2\sigma U_\mu H, \quad \delta = \frac{\mu U_\mu}{2\sigma}h. \tag{5}$$

Using typical values from table 1, we find that $\delta \simeq 10h \simeq 1.5\,\mathrm{mm} \ll H$ and $\delta \gg h$. Notice that Culick's (1959) estimation of δ in soap films gives $\delta \simeq 0.2h$. Therefore, whereas in low-viscosity soap films the transition zone is quite small ($\delta \simeq 0.2h$), it is quite large in the thick viscous films considered here ($\delta \simeq 10h$). This is completely in line with usual intuition about viscous flows, and differs only by a factor of 2 from the result of Culick (1960), and is not an unexpected result. This also completely agrees with results of numerical simulations by Brenner & Gueyffier (1999). In addition, Sünderhauf *et al.* (2002) explicitly demonstrated that the rim extends into the film on a distance proportional to capillary number *Ca* (inverse of their Γ_v parameter, p. 199; see fitting parameter c on figure 5, p. 201, and derivation on p. 202).

Notice, however, that though in our system the size of the viscous transition zone δ is about one order of magnitude larger than h, it is about one order of magnitude smaller than H. Therefore, we can use a consideration similar to that from the dimensional analysis above which leads to the Taylor–Culick formula, (1). Namely, near the centre between the needles, the distance to the needles is of the order of $H/2 \gg \delta$. This means that at distance δ from the rim near the centre between the needles, the film thickness is very close to h, and pressure is very close to constant atmospheric pressure. Therefore, locally, in the centre between the needles, the liquid particles propagate as if they are 'unaware' of the external size of the system H. We can use therefore the *initial rupture stage*, when the expanding rim from the puncture in the middle between the needles just reached the needles, as a model for the rim during the entire motion. We assume therefore that we can approximate the front of the rupture by a thin half-torus of diameter H and cross-sectional radius r. Therefore, for the purposes of gross mass balance and estimation of rim thickness r, we can assume that the mass of the uniform film from the semicircle between the needles, $(1/2)\pi(H/2)^2h\rho$, is concentrated in the thin semi-torus rim of cross-sectional radius r between the needles. Using the formula for the mass of the thin half-torus $(\pi H/2)\pi r^2\rho$, we obtain:

$$\frac{1}{2}\frac{\pi H^2}{4}h = \frac{\pi H}{2}\pi r^2, \quad r = \frac{1}{(4\pi)^{1/2}}(Hh)^{1/2}. \tag{6}$$

Using (6) for evaluating r, with typical values $H = 1.6\,\mathrm{cm}$ and $h = 0.15\,\mathrm{mm}$, we derive $r \simeq 0.43\,\mathrm{mm}$. This means that $r \simeq 3h$ and the rim thickness $2r$ is of the order of $6h$. It was difficult to measure the rim thickness through the processing of the digital images owing to the high curvature of the rim surface and its relatively small width. Nevertheless, it was clear both from the visual observations of the experiment and digital images, that the rim is a few times thicker than the film itself.

At the same time, δ is of the same order, or somewhat larger, than r. This shows that the transition zone in front of the rim contains a liquid amount which is not negligible in comparison with the 'quasi-circular' rim. However, derivation of (6) assumed that the rim contains all of the liquid from the semicircle. This shows that approximation (6) is in fact quite crude. Nevertheless, being conceptually simple, without adjustable parameters, and derived from first principles, expression (6) has its own merit. In spite of its crude nature, it is used below for the evaluation of forces balance.

Notice that near the needles, the reasoning that led to the derivation of (6) is not applicable. When the rim approaches the needles (when the distance from the rim to the needles is of order δ), conservation of mass leads to the thickening of the rim compared to r. Indeed, assume that at the last stage of the flow, the entire mass of the ruptured film is concentrated in two uniform circular rims of cross-sectional radius $\bar{r}$ near the needles. Equating the volume of the initial quiescent film per unit length along the needles Hh, and the volume of the rims of radius $\bar{r}$ per unit length at the final stage near two needles $2\pi\bar{r}^2$ yields:

$$2\pi\bar{r}^2 = Hh, \quad \bar{r} = \frac{1}{(2\pi)^{1/2}}(Hh)^{1/2}. \tag{7}$$

As may be seen, $\bar{r}$ is indeed larger than r, though of the same order.

3.3. *Asymptotic force balance*

To find the rim propagation velocity U_μ, let us consider the forces acting on the rim element. To estimate viscous forces, notice that overall, the rupture dynamics is unidirectional. Hence, we assume that in the steady-state mode the surface tension forces on the edge of the rupture are balanced by the viscous shear forces, while the inertia of the rim is neglected.

To evaluate the viscous shear forces we notice that the liquid is immobile on the needles ($x = \pm H/2$). At the same time, the liquid at the centre of the front moves with velocity U_μ. So, the velocity gradient is of order $2U_\mu/H$, therefore the viscous stress is of order $2\mu U_\mu/H$.

As for the surface tension, we assume that the rim has a quasi-circular cross-sectional profile (see figure 3). Notice that $\delta \simeq 10h$ and $2r \simeq 6h$ (diameter of the rim) are of the same order. This suggests that the quasi-circular cross-sectional profile assumption, though not ideal, is roughly correct. Also, the results of numerical simulations and shapes of the rim, shown by Sünderhauf *et al.* (2002) support such an assumption. We might expect that for the crude averaged force balance, the quasi-circular cross-sectional profile of the rim would be a reasonable approximation.

Notice that the film is thin and $r \ll H$, therefore the curvature across the rim is dominant. So, the surface tension stress is of the order of σ/r. Balancing viscous and capillary stresses, we obtain

$$2\mu\frac{U_\mu}{H} = \frac{\sigma}{r}, \quad U_\mu = \frac{\sigma}{2\mu}\frac{H}{r}. \tag{8}$$

Substitution of r from (6) yields:

$$U_\mu = \pi^{1/2}\frac{\sigma}{\mu}\left(\frac{H}{h}\right)^{1/2}. \tag{9}$$

Equation (9) gives an asymptotic value of the rupture velocity on the assumption of negligible inertia. Table 1 presents the results of the theoretically obtained values of U_μ from (9) in comparison with the velocity measurements. Though the analysis

leading to (9) is crude, it gives good results. At the same time, for the typical thickness $h = 0.15\,\text{mm}$, the Taylor–Culick velocity U_{TC}, given by (1), is equal to $67\,\text{cm}\,\text{s}^{-1}$. All the velocities, observed in our experiments, are rather lower than this value. This fact and the agreement between theoretical and experimental velocity values corroborate the assumption of negligible inertia.

Using (9), we obtain $\delta = \pi r$; the observation that δ and r are of the same order was mentioned before. So, the derivation above led to the self-consistent theory.

Now let us consider the Reynolds number Re of our system. Notice that the film far from the rim remains motionless. We consider δ as a characteristic 'intrinsic' length scale. Using (9) and (5), the expression for the Reynolds number $Re = \rho U_\mu \delta/\mu$ yields:

$$Re = \frac{\rho\pi\sigma H}{2\mu^2} = \frac{U_\mu^2}{U_{TC}^2}. \tag{10}$$

From (10), we see that the Reynolds number of the system does not depend on the film thickness h. This is becuase both U_{TC} and U_μ are inversely proportional to $h^{1/2}$. As might be expected, the Reynolds numbers for our system are smaller than 1 (see table 1).

3.4. *Full balance of forces*

In the experiments conducted in the present study, viscosity and surface tension control the flow. It is worth, nevertheless, considering the rupture of a low-viscosity film between two parallel needles, when inertia is significant. This would correspond to the rupture of, say, soap films between the needles. We assume that the rupture propagates in a steady mode (as was found by Liebman *et al.* 1968), but the velocity U is different from that of the viscosity dominated regime U_μ. The dynamic equilibrium between mass accumulation on the rim and mass retention on the needles allows us to close the problem. Evaluation of the rim radius r in § 3.1 was based on kinematic considerations and was independent of the nature of the forces in our system. Therefore, we adopt (6) for the rim radius r in our analysis of full forces balance.

To derive momentum balance, consider the dynamics of the liquid particles on the rim in detail, similar to that by Taylor (1959) and Culick (1960). After being absorbed by the rim, the liquid particle begins to move with velocity U and then slips away along the rim towards the needle. Therefore, the flow area near the rim may be considered as consisting of two areas: at the centre between the needles the liquid particles acquire momentum, while the area near the needle is the sink of slowly moving mass with negligible momentum. This allows us to use averaged momentum balance on the rim to find U.

Gross momentum increment $\mathrm{d}[MU]$ of the front edge of the rim during time $\mathrm{d}t$ is approximately equal to:

$$\mathrm{d}[MU] = U\,\mathrm{d}M = \rho H h U^2\,\mathrm{d}t, \tag{11}$$

where $\mathrm{d}M = \rho H h U\,\mathrm{d}t$ is the mass increment of newly absorbed moving liquid, $U = const$. Therefore, in the spirit of Taylor (1959), conservation of averaged momentum for the steady-state mode in the cross-sectional plane perpendicular to the needles gives:

$$F_\sigma\,\mathrm{d}t = \mathrm{d}[MU] + F_\mu\,\mathrm{d}t, \tag{12}$$

$$F_\sigma = 2\sigma H, \quad F_\mu = 4\mu U r. \tag{13}$$

Here, F_σ and F_μ are the gross forces due to the surface tension and viscosity, respectively. Both F_σ and F_μ are obtained by multiplication of stresses in (8) by the

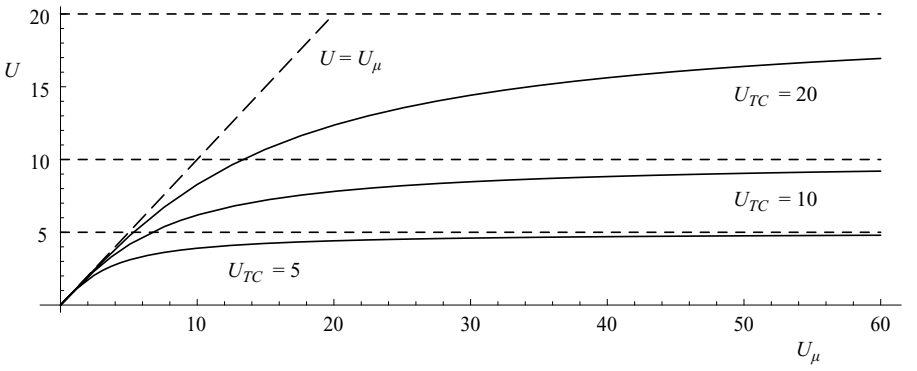

FIGURE 4. U as a function of U_μ for $U_{TC} = 5, 10, 20$.

crude expression for the cross-sectional area on the front of the rim $2rH$. Substitution of (13) and (11) into (12) yields:

$$\frac{2\sigma}{\rho h} = U^2 + \frac{4\mu r}{\rho H h}U, \quad 1 = \left(\frac{U}{U_{TC}}\right)^2 + \frac{U}{U_\mu}. \tag{14}$$

Expression (14) is valid both for small and large viscosities of the film. Simple analysis of equation (14) shows that $U \to U_{TC}$ as $U_\mu \to \infty$, and $U \to U_\mu$ as $U_{TC} \to \infty$. This is illustrated by figure 4. In the case of large μ, velocity U_μ is small, the first inertial term in the right-hand side of (14) is negligible, and the asymptotic expression for viscosity dominated regime (8) is recovered. For small values of μ, velocity U_μ is large, the second viscous term in the right-hand side of (14) is dropped, and we derive the Taylor–Culick formula, (1), for the rim velocity.

Equation (14) gives the expression for U as a function of U_μ and U_{TC} through the system parameters h, H, σ, ρ, μ. Solutions of (14) are shown in figure 4. Here we do not consider the negative root of U, since it has no physical meaning.

Note that the classic theory of Taylor and Culick describes asymptotic values of U shown as horizontal lines in figure 4. At the same time, (8) describes the straight-line asymptotics near the origin in figure 4. It would be interesting to conduct experiments on a broad range of viscosities and film thicknesses to evaluate equation (14).

Notice, however, the important difference between the rupture process in the previous studies and between the needles. Generally speaking, in all the previous papers, the rim collects all the liquid of the film, and the film itself is not constrained. As a result, the rim thickness grows in time. This is true both for axisymmetric geometry and a one-dimensional film contraction, as considered by Brenner & Gueyffier (1999). In contrast to that, in the film rupture between the needles, the rim thickness does not grow in time owing to dynamic mass retention on the needles (see § 2). At the same time, the needles act as solid boundaries and restrain the propagation velocity of the rim.

On the other side, long bubble propagation considered by Bretherton (1961) is also different from our system because the liquid between the bubble and the tube walls is conserved, and cannot be 'squeezed out'. Unlike that, in our system, liquid is accumulated on the needles, and is effectively 'squeezed out' into an additional dimension perpendicular to the plane of the film. The same argument applies to the finger propagation studied by Saffman & Taylor (1958). The liquid between the

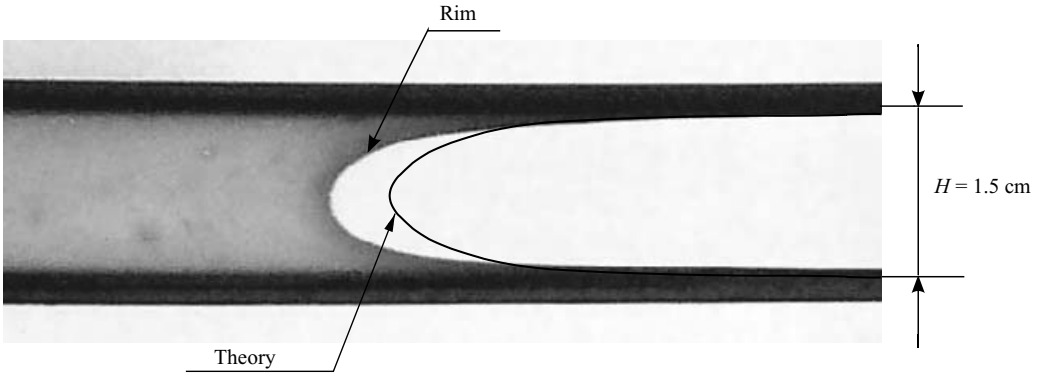

FIGURE 5. Comparison of experimental U-shaped profiles with crude theory for viscosity dominated regime, $U/U_{TC} = 0$.

walls and the finger is conserved, and cannot be 'squeezed out' into an additional dimension. This is why the comparisons of our system with well-known classic flows bring only limited insight into the rupture dynamics.

3.5. *U-shaped profile for viscous case: crude theory*

Our system reaches steady-state propagation mode with constant velocity U_μ. It allows us to propose a crude theory for the instantaneous profile $y(x)$ of the rupturing film. Conceptually, we will use the same forces balance as above. In addition, in an obvious stretch of its averaged nature and in its applicability, we will apply averaged considerations locally to every element of the rim.

Consider the normal velocity U_n of the rim particles, which have components in both the x- and y-directions. Since the y-component of velocity is equal to U_μ for all particles, the expression for U_n reads:

$$U_n = \frac{U_\mu}{(1 + y'^2)^{1/2}}. \tag{15}$$

The system is symmetric with respect to the centreline between the needles. Thus, consider the case $x \geqslant 0$. The liquid at the needle ($x = H/2$) is immobile, whereas at $(x, y(x))$ it moves with velocity U_n, defined by (15). So, the velocity gradient for the liquid particles on the rim can be written as $U_n/(H/2 - x)$, $0 \leqslant x < H/2$. The film is thin and $r \ll H$. Therefore, we can make a crude assumption that the asymptotic forces balance for the viscosity controlled regime (8) remains valid. Consequently, we shall use the normal velocity U_n and distance $H/2 - x$ instead of U_μ and $H/2$, respectively, to define velocity gradient. Thus, (8) takes form:

$$\mu \frac{U_n}{H/2 - x} = \frac{\sigma}{r}. \tag{16}$$

Substitution of (8) and (15) into (16) yields:

$$\frac{H/2}{H/2 - x} = (1 + y'^2)^{1/2}. \tag{17}$$

Here, the exact solution of (17) is not pursued. For $x \to H/2$, $0 \leqslant x < H/2$, the asymptotic solution of (17) has the form $y(x) \simeq (H/2)\log(1/|x - H/2|)$. Comparison of the numerical solution of (17) with the experimental profile is presented in figure 5.

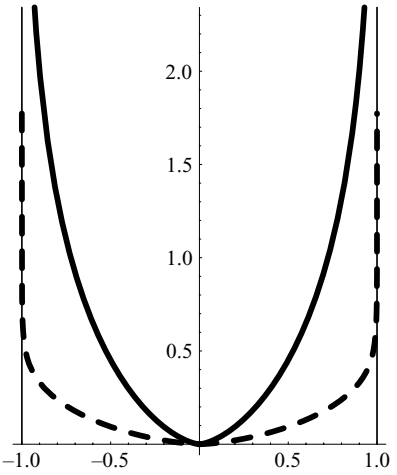

FIGURE 6. U-shaped profiles: solid curve – for viscosity dominated regime, $U/U_{TC}=0$; dashed curve – for inertial regime, $U/U_{TC}=0.9$.

To be visible on the picture, the numerical solution (solid line) is shifted with respect to the profile. Overall, the solid curve in figure 5 corresponds reasonably well to the observed U-shaped rupture profile, in spite of the crude nature of model (17). However, the very 'nose' of the numerical profile is somewhat sharper that the experimentally observed profiles.

3.6. *U-shaped profile for inertial regime: crude theory*

The previous section presented a crude theory for the U-shaped profile in the viscous regime. The essence of the theory is quite crude. Nevertheless, it seems that it might be instructive to apply the same approach to evaluation of the rupture profile $y(x)$ when inertia is significant (not studied experimentally in the present paper). Although crude, the approach might provide some insight into the structure of the U-shaped profile in the inertial regime.

We shall use the forces balance (14) and expression (15) in the same fashion as above. We replace U by its normal component $U_n=U/(1+y'^2)^{1/2}$. The inertial component of (14) does not depend on x. Note, however, that irrespective of the value of the Reynolds number, the viscous forces near the needles ($x\to\pm H/2$) become dominant. At the same time, in the second term of (14), the ratio U_μ/U_n takes the form $U_n/(U_\mu(1-2x/H))$ owing to the viscous impact on the needles. Thus, we recast the forces balance (14) in the following form:

$$1=\left(\frac{U_n}{U_{TC}}\right)^2+\frac{U_n}{U_\mu(1-2x/H)}. \tag{18}$$

Equations (17) and (18) should be regarded as merely 'methaphorical' (we owe this description to one of the referees). Their crude nature is obvious. Still, their solution may provide some guidance and insight into the impact of inertia on the U-shaped rupture profile.

The numerical solution of (18) is shown by a dashed line in figure 6. The rupture profile in the inertia-dominated regime has a more flattened form, compared to that for the viscous case. It would be tempting to conduct experiments on the rupture of thin films less viscous than those considered in the present paper to ascertain the validity of (18).

4. Conclusion

The rupture of viscous films between two parallel needles has been considered. The Reynolds number of the system lies in the range $0.002 \leqslant Re \leqslant 0.34$. It has been shown that the obtained asymptotic rim velocity (9) agrees well with the experimental data. The rim thickness of the film has also been theoretically estimated, although its measurements were not made. A model for the U-shaped rupture profile has been proposed. The method of analysis is based on the crude forces balance, and leads to the expression (14), valid for both low and high viscosities. The classic result, (1), by Taylor and Culick is recovered in the case when inertia is significant. Since the full model has not been compared to experiments, it would be interesting to verify the theory for velocity and the U-shaped rim profile in a broader range of liquid viscosities and films thicknesses.

We are grateful to Tim Endres and Jeff Allen for their help in conducting the experiments. We are deeply indebted to the referees, whose numerous comments improved the paper in many critical aspects. This material is based upon work supported by the National Science Foundation under Grant 0325743. Our thanks also go to BP Amogo Chemicals for kindly providing the Indopol polybutene.

REFERENCES

Adachi, K., Aoki, T., Nishida, S. & Nakamura, R. 1988 A hydrodynamic investigation of a falling liquid film for curtain coating and sheet casting. *Xth International Congress on Rheology, Sydney*, vol. 1, p. 122.

Barenblatt, G. I. 1996 *Scaling, Self-similarity, and Intermediate Asymptotics: Dimensional Analysis and Intermediate Asymptotics*. Cambridge University Press.

Brenner, M. P. & Gueyffier, D. 1999 On the bursting of viscous films. *Phys. Fluids* **11**, 737.

Bretherton, F. P. 1961 The motion of long bubbles in tubes. *J. Fluid Mech.* **10**, 1961.

Culick, F. E. C. 1960 Comments on a ruptured soap film. *J. Appl. Phys.* **31**, 1128.

Debrégeas, G., Martin, P. & Brochard-Wyart, F. 1995 Viscous bursting of suspended films. *Phys. Rev. Lett.* **75**, 3886.

Debrégeas, G., de Gennes, P.-G. & Brochard-Wyart, F. 1998 The life and death of bare viscous bubbles. *Science* **279**, 1704.

Dupré, A. 1867 Theorie Mécanique de la Chaleur. *Ann. Chim. Phys.* **(4) 11**, 194.

Keller, J. B. 1983 Breaking of liquid films and threads. *Phys. Fluids* **26**, 3451.

Landau, L. D. & Lifshitz, E. M. 1959 *Fluid Mechanics*. Pergamon.

Liebman, I., Corry, J. & Pierlee, H. E. 1968 Rupture mechanism of a liquid film. *Science* **161**, 373.

McEntee, W. R. & Mysels, K. J. 1969 The bursting of soap films. I. An experimental study. *J. Phys. Chem.* **73**, 3018.

Pandit, A. B. & Davidson, J. F. 1990 Hydrodynamics of the rupture of thin liquid films. *J. Fluid Mech.* **212**, 11–24.

Ranz, W. E. 1959 Some experiments on the dynamics of liquid films. *J. Appl. Phys.* **30**, 1950.

Rayleigh, Lord 1891 Some applications of photography. *Nature* **44**, 249. (Also *Scientific Papers*, vol. 3, 1898, p. 441.)

Saffman, P. G. & Taylor, G. I. 1958 The penetration of a fluid into a porous medium of Hele-Shaw cell containing a more viscous liquid. *Proc. R. Soc. Lond.* A **245**, 312.

Sünderhauf, G., Raszillier, H. & Durst, F. 2002 The retraction of the edge of a planar liquid sheet. *Phys. Fluids* **14**, 198.

Taylor, G. I. 1959 The dynamics of thin sheets of fluid. III. Disintegration of fluid sheets. *Proc. R. Soc. Lond.* A **253**, 313. (Also *Scientific Papers of G. I. Taylor*, vol. 4, 1971, p. 368.)

Vorobieff, P., Rivera, M. & Ecke, R. E. 1999 Soap film flows: statistics of two-dimensional turbulence. *Phys. Fluids* **11**, 2167.